ChemistrySelect

Research Article
doi.org/10.1002/slct.202501478

Chemistry Europe
European Chemical Societies Publishing

www.chemistryselect.org

Effect of Fe_3O_4 Nanoparticles on Lovastatin Drug Release from Chitosan Films

Vu Quoc Manh,[a] Tran Minh Thi,[b, c] Doan Thi Yen,[d] Nguyen Thuy Chinh,[e, f] Nguyen Thi Hong Nhung,[a] Nguyen Ngoc Linh,[a] Ly Thi Ngoc Lien,[e, f] Thai Hoang,[e, f] Nguyen Thi Bich Viet,[d] Vu Thi Huong,[d] Nguyen Dang Dat,[d] Ha Manh Hung,[g] and Vu Quoc Trung*[d]

Fe_3O_4 nanoparticles, known for their biocompatibility can be combined with chitosan and PEG—biocompatible and biodegradable polymers—as well as lovastatin to create targeted drug delivery systems. The chemical structure, composition, morphology, and magnetic properties of the composite films were analyzed using Fourier transform infrared (FTIR) spectroscopy, energy-dispersive X-ray (EDX) mapping, field emission scanning electron microscopy (FESEM), and a vibrating sample magnetometer (VSM). The results showed that lovastatin was well dispersed within the chitosan matrix, with particle sizes ranging from 10 to 40 μm, while Fe_3O_4 nanoparticles exhibited a tendency to agglomerate. The release of lovastatin from the composite films in simulated body fluids (pH between 2.0 and 7.4 buffer solutions) was studied using ultraviolet-visible (UV–vis) spectroscopy. The drug release was found to depend on environmental pH, Fe_3O_4 nanoparticle content, and testing time. These findings suggest the potential of this system for targeted drug delivery applications.

1. Introduction

Cholesterol plays a vital role in the formation of cell membranes, and acts as a precursor in the synthesis of vitamin D and other hormones.[1,2] However, the excess cholesterol in the vascular system will be harmful to the body, causing many diseases related to heart disease, dyslipidemia, atherosclerosis, myocardial infarction, etc.[3]

Currently, many statin drugs such as atorvastatin, fluvastatin, lovastatin, pravastatin, etc are often used to lower blood cholesterol. Among them, lovastatin (Lov) is a commonly used drug with high efficacy and low toxicity. Lov prevents cholesterol formation by inhibiting the enzyme hydroxymethylglutaryl coenzyme A reductase (HMG-CoAR).[4] In addition, Lov reduces low-density lipoprotein (LDL) and increases high-density lipoprotein.[5] However, a major drawback of Lov that limits its therapeutic application is that the bioavailability of Lov is quite low and unstable due to its low water solubility.[6–9]

Recent research has focused on using naturally occurring polymers, particularly polysaccharides such as chitosan, starch, alginate, and collagen to enhance drug bioavailability. Studies by A. C. Tiryaki et al. and H. Thai et al. have demonstrated the effectiveness of these materials in controlling the release of lovastatin and ginsenoside RB1 in body fluids, improving their therapeutic potential.[10–12] In another study, alginate/chitosan nanocarriers were developed and optimized to simultaneously deliver two antibiotics, doxycycline and florfenicol, along with silver nanoparticles.[13] However, there are many studies on the physical-chemical properties, drug delivery and release properties of composite materials of Fe_3O_4, polymers and the functional groups of chitosan, lovastatin. Fe_3O_4 nanoparticles are of great interest and are ideal candidates for applications in drug delivery, radiation therapy thermography, cell sorting, magnetic resonance imaging (MRI), immunoassay and separation, purification of biomedical products, anticancer drug delivery,[14–16] radiotherapy-related applications.[17–19] However, their high surface area-to-ume ratio and hydrophobic surfaces often cause them to aggregate, forming large clusters. To overcome this issue, iron oxide nanoparticles are commonly coated with biocompatible substances such as chitosan,[20] dextran,[21] alginate,[22] poly(ethylene glycol),[23] and polyvinylpyrrolidone.[15,24–26]

Polyethylene glycol (PEG)-based biomaterials are highly water-soluble, exhibit excellent biocompatibility and do not stimulate an immune response. Additionally, PEG has been

[a] Dr. V. Q. Manh, N. T. Hong Nhung, Dr. N. N. Linh
Institute of Medicine and Pharmacy, Thanh Do University, Hoai Duc, Ha Noi 100000, Vietnam

[b] Prof. T. M. Thi
Institute of Theoretical and Applied Research, Duy Tan University, Hanoi 100000, Vietnam

[c] Prof. T. M. Thi
Faculty of Nature Science, Duy Tan University, Da Nang 550000, Vietnam

[d] D. T. Yen, Dr. N. T. Bich Viet, Dr. V. T. Huong, Dr. N. D. Dat, Prof. V. Q. Trung
Faculty of Chemistry, Hanoi National University of Education, 136 Xuan Thuy, Cau Giay, Ha Noi 100000, Vietnam
E-mail: trungvq@hnue.edu.vn

[e] Prof. N. T. Chinh, L. T. Ngoc Lien, Prof. T. Hoang
Institute of Materials Science, Vietnam Academy of Science and Technology, 18 Hoang Quoc Viet, Nghia Do, Hanoi 100000, Vietnam

[f] Prof. N. T. Chinh, L. T. Ngoc Lien, Prof. T. Hoang
Graduate University of Science and Technology, Vietnam Academy of Science and Technology, 18 Hoang Quoc Viet, Nghia Do, Ha Noi 100000, Vietnam

[g] Dr. H. M. Hung
Faculty of General Education, Ha Noi University of Mining and Geology, Duc Thang, Dong Ngac, Ha Noi 100000, Vietnam

shown to enhance stability during internal body circulation.[27] When used as a water-swelling hydrogel, PEG-based hydrogel nanoparticles can be precisely tuned in size to improve permeability and retention effects (PRE), thereby optimizing the drug release mechanism.[27–29]

Lovastatin (Lov), a cholesterol-lowering drug, was selected as the model drug due to its well-established therapeutic benefits in treating hypercholesterolemia. However, its low aqueous solubility and rapid metabolism in the gut and liver result in poor oral bioavailability (less than 5%) and a short half-life of 1–2 h.[30–33] Therefore, further studies are needed to develop a formulation that enhances oral absorption and enables extended drug release.

The research on the release of chitosan, lovastatin from PEG containing drugs,[34,35] Fe_3O_4 containing drug,[45] the role of Fe_3O_4,[36–42] the drug release mechanism[40–42] containing Fe_3O_4 are also interesting. Several studies have observed drug release in various pH environments (pH: 2.0, 4.5, 5.0, 6.5, 6.8, and 7.4), yielding highly variable results. However, there are still very few studies investigating composite materials incorporating nanomagnetic Fe_3O_4, PEG[28,29,34–36] and chitosan in lovastatin drug release[12,33,45] in the pH 2, pH 7.4 environment of the stomach and small intestine

In this work, we focus on investigating magnetic Fe_3O_4 nanoparticles with the ability to be distribute by an external magnetic field, chitosan as the drug carrier, PEG as good biocompatibility, and lovastatin as the treatment drug. These issues are important as it allows for the development of a multifunctional drug delivery platform that can potentially improve the targeted delivery and controlled release of therapeutics through the use of Fe_3O_4 nanoparticles. Therefore, this study aimed to (i) prepare the thin films based on chitosan as a drug carrier, Fe_3O_4 nanoparticles, and lovastatin as a treatment drug, (ii) investigate the characteristics as well as evaluate the effects of ferromagnetic nanoparticles on the ability to control and release lovastatin from these thin films between pH 2.0 and pH 7.4 simulated body fluids.

2. Materials and Methods

2.1. Materials

Polyethylene glycol 4000 (PEG, purity $\geq$ 98.0%) and lovastatin (purity $\geq$ 98.0%) were provided by Sigma Aldrich. Chitosan has a deacetylation degree $>$ 75%–85% and a polymer density index of 1.61×105 Da (Sigma Aldrich). Other chemicals such as KCl, NaOH, KH_2PO4, HCl 37%, Na_2SO_3, $FeCl_3$. $6H_2O$, NH_3, CH_3COOH 99.5%, ethanol, distilled water, and acetone 99% were purchased from Sigma Aldrich and used without further purification.

2.2. Synthesis of Fe_3O_4 Nanoparticles

$FeCl_3$. $6H_2O$ (20.25 g) was dissolved in 100 mL of distilled water, then 0.85 mL of 1 M HCl solution was added and stirred to obtain a yellow-brown solution **S1**. The HCl solution creates an acidic environment that facilitates the reduction from Fe^{3+} to Fe^{2+} by the reducing agent Na_2SO_3. Na_2SO_3 (1.575 g) was dissolved in 50 mL of distilled water to obtain solution **S2**. The mixture of solutions **S1** and **S2** was stirred for 30 min until the solution turned bright yellow to get solution **S3**. The pH was then adjusted to 9–10 by slowly adding NH_3 to solution S3 and then stirred for 30 min at 80 °C to obtain a black mixture that needs to be filtered by a magnet. The resulting mixture bottle was placed on a magnetic substrate for the Fe_3O_4 nanoparticles to settle rapidly. After decantation, Fe_3O_4 nanoparticles were filtered and washed 3 times with distilled water and 2 times with acetone. The raw product was dried at 50 °C for 1 day and finely ground to achieve black Fe_3O_4 nanoparticles.

Table 1. Composition of CFL samples.

Composite sample	% w/w (Fe_3O_4/CS)	CS (g)	Lov (g)	PEG (g)	Fe_3O_4 (g)
CFL0	0	0.5	0.025	0.05	0
CFL5	5	0.5	0.025	0.05	0.025
CFL10	10	0.5	0.025	0.05	0.050
CFL15	15	0.5	0.025	0.05	0.075
CFL20	20	0.5	0.025	0.05	0.100

2.3. Synthesis of Chitosan/Fe_3O_4/Lovastatin (CFL)

An amount of 0.5 g of chitosan (CS) was dissolved in 50 mL of 1% acetic acid solution to obtain solution **A**. 0.025 g of lovastatin was dissolved in 10 mL of ethanol to obtain solution **B**. 0.05 grams of PEG was dissolved in 5 mL of distilled water to obtain solution **C**. Solution **C** was mixed with different amounts of Fe_3O_4 (as shown in Table 1) by ultrasonically shaking to obtain solutions **D**. The mixture of solutions **A** and **B** was ultrasonically stirred at 18,000 rpm and stirred continuously for 60 min to obtain solution **E**. Solution **D** was slowly added to solution **E** and sonicated for 60 min. The resulting solution was poured into a petri dish for natural evaporation to obtain CFL composite films with a thickness of 0. 1 $\pm$ 0.001 mm. The thin composite films with Fe_3O_4 contents of 0, 0 025, 0 050, 0 075, and 0 100 g per 0 5 g of chitosan were denoted as **CFL0**, **CFL5**, **CFL10**, **CFL15**, and **CFL20**, respectively.

2.4. Characterization

Transform Fourier Infrared (FTIR) spectra of chitosan/Fe_3O_4/lovastatin (CFL) films were recorded using a Nicolet/Nexus 670 Spectrometer (American) at room temperature with 32 scans at 8 cm^{-1} resolution and in the wavelength region of 400 cm^{-1} - 4000 cm^{-1}. Field Emission Scanning electron microscope (FE-SEM) analysis of CFL films was performed using a Hitachi S-4800 FE-SEM. UV–vis spectra were recorded on a GBC Cintra 40 UV–visible spectrophotometer to determine the concentration of Lov released from CFL composites in different

pH environments. Energy-dispersive X-ray (EDX) spectroscopy was measured by a 6000E-HTEK EDX (China). The magnetic properties of samples were measured by a vibrating sample magnetometer (VSM). Differential Scanning Calorimetry (DSC) of CFL films was performed using a NETZSCH DSC 204F1. Thermogravimetric analysis or thermal gravimetric analysis (TGA) of CFL films was performed using a Labsys TGA 1600 Setaram. X-ray diffraction analysis (XRD) of CFL films was performed using a D8 Advance, Bruker, Germany, CuK-alpha 40 kV 40 mA generator, NaI scintillation detector. Cell proliferation inhibitory activity assay, MTT ([3-(4,5-dimethylthiazol-2-yl)-2,5-diphenyltetrazolium bromide]) method was carried out on Vero cell of CFL films. The mechanical properties of films were tested on Zwick 2.5 testing machine (Germany) according to ASTM D882.

2.5. Release of Drugs

In this study, the release process of Lov from CFL films was carried out in simulated intestinal fluid (pH 7.4 phosphate-buffered saline, PBS) and simulated gastric fluid (pH 2.0 HCl/KCl buffer). The study of Lov release from CFL films was performed as follows: 15 mg of each CFL sample was immersed in 100 mL of pH 7.4 PBS and pH 2.0 buffer, respectively, then incubated at 37 °C on a rotary shaker at 120 rpm. After every hour of shaking, 5 mL of solution was withdrawn to monitor the released Lov concentration by the UV–vis spectrophotometer. Fresh buffer solutions were added accordingly after each withdrawal to maintain the total ume. The drug release was monitored for over 28 h. The percentage of Lov released (T%) was determined by the following equation:

$$\%T = \frac{m_t}{m_0}.100$$

where m_0 and m_t are the amounts of Lov in the original sample and the amount of Lov released at time t, respectively. All experiments were performed in duplicate three times.

2.6. Drug Release Kinetics

There are different kinetics and drug release mechanisms based on polymeric substrates.[40–42,45,46] Release of drug from polymeric substrates is usually due to penetration of water in the matrix, hydration, swelling, diffusion of the soluble drug, or disintegration of the polymer layer.[40] The mechanism of drug release depends on the dose of the drug, the pH of the solution, the nature of the drug, and the polymer used. Recently, several kinetic models have been used to study drug release as follows:[12,44–46]

$$\text{Zero} - \text{orderkinetics (ZO)} : \rightarrow W_t = W_0 + k_1.t \quad (1)$$

$$\text{First} - \text{orderkinetics (FO)} : \rightarrow \log C_t = \log C_0 - k_2.t/2.303 \quad (2)$$

$$\text{Hixson} - \text{Crowell (HCW)} : (100 - W)^{1/3} = 100^{1/3} - k_3.t \quad (3)$$

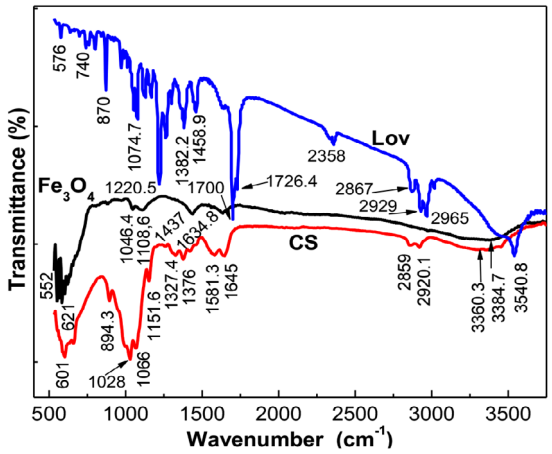

Figure 1. IR spectra of pure Fe_3O_4, CS, and Lov.

$$\text{Higuchi (HG)} : W_t = k_4.t^{1/2} \quad (4)$$

$$\text{Korsmeyer} - \text{Peppas (KMP)} : \; M_t/M_\infty = k_5.t^n \quad (5)$$

where k_i is the drug release constant; C_t and C_0 are drug concentrations at the testing time and at the initial time, respectively; W_t and W_0 are the mass of the drug at the testing time and at the initial time, respectively; M_t/M_∞ is the fraction of drug released into the dissolution medium; n is the diffusion constant.

The kinetics data of Lov release from CFL films were calculated according to the above five kinetic equations.

3. Results and Discussion

3.1. FT-IR Spectra of CFL Films

The FTIR spectra of pure CS, Lov, and Fe_3O_4 are presented in Figure 1. In addition to the characteristic bands of –CH vibration at 2920 cm^{-1}, C–O vibration at 1068 cm^{-1}, the CS spectrum exhibits strong bands at 3360 cm^{-1} of –OH and $–NH_2$ vibrations. Moreover, the FTIR spectrum of CS also has the vibrations of the $–NH_2$ bond at 1581 cm^{-1}, vibrations of the saccharide ring at 894 cm^{-1}, and vibrations of the C═O bond at 1646 cm^{-1}.[34]

The FTIR spectrum of Lov shows characteristic bands of the valence vibrations of the –OH bond at 3544 cm^{-1}. Three bands at 2965 cm^{-1}, 2929 cm^{-1}, and 2867 cm^{-1} are attributed to vibration of CH_3, CH_2, and saturated CH bond, respectively. The strong band at 1700 cm^{-1} is characteristic of the vibration of the C═C bond while the 1726 cm^{-1} and 1074 cm^{-1} bands are attributed to the vibrations of the C═O and –C–O–C bonds, respectively.[35]

In the FTIR spectrum of Fe_3O_4, the characteristic vibrations of the Fe–O bond appear between 552 cm^{-1} and 583 cm^{-1}. In addition, there are stretching vibrations and deformation vibrations of the –OH group of water adsorbed on the Fe_3O_4 surface appearing between 3384 cm^{-1} and 1634 cm^{-1}, respectively.[35]

The FTIR spectra of CFL composite films with different Fe_3O_4 contents (0%–20% by weight of CS) are presented in Figure 2. All

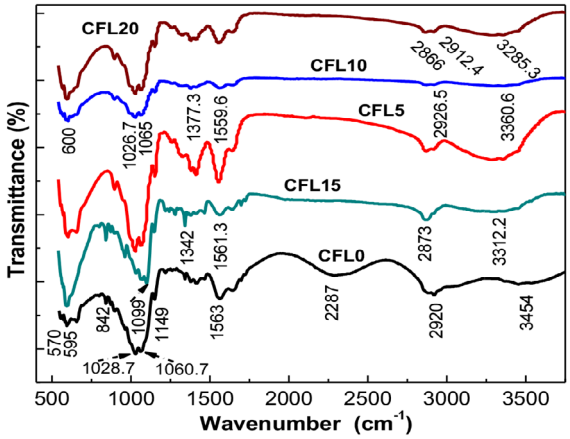

Figure 2. FTIR spectra of CFL films with various Fe_3O_4 contents (0% – 20%).

Table 2. Major vibrations in FTIR spectra and saturation magnetization of CFL films.

Composite sample	Wavelength (cm^{-1})						Saturation magnetization, M_S (emu/g)
	$\nu_{-NH2,\ -OH}$	ν_{CH}	$\nu_{C=O}$	δ_{NH2}	ν_{C-O-C}	ν_{FeO}	
CFL0	3454	2919	1651	1414	1060	–	–
CFL5	3364	2868	1642	1410	1066	601	2.6
CFL10	3360	2869	1650	1377	1065	535	4.96
CFL15	3312	2872	1651	1417	1075	594	7.9
CFL20	3357	2865	1651	1417	1064	570	10.8

the characteristic vibrations in CS, Fe_3O_4, and Lov components appear in the FTIR spectra of the CFL composite films. There are some small shifts in the peaks corresponding to the characteristic bands of CS, Fe_3O_4, and Lov in the CFL composite film compared to each original component. This can be explained by the fact that CS, Fe_3O_4, and Lov have strong interactions with each other by dipole-dipole interactions and hydrogen bonds between the amine groups of CS and the hydroxy of Lov. However, the characteristic bands for the corresponding groups in the CFL composite films hardly change when changing the Fe_3O_4 concentration. Thus, the Fe_3O_4 concentration did not affect the interaction between Lov and CS.

The MS values and magnetization curves obtained with CFL films are presented in Table 2 and Figure 3. This result demonstrates the participation of Fe_3O_4 at different concentrations in the samples.[36–39] Figure 3 shows that all the samples are superparamagnetic with the saturation magnetization MS increasing proportionally to the Fe_3O_4 content in the samples, from 2.6 to 10.8 emu/g in a magnetic field H of 10,000 Oe. This superparamagnetic behavior is desirable as an external magnetic field can easily manipulate the samples without retaining any magnetization once removed. More specifically, they can be controlled to tag biomolecules magnetically, enabling precise command over their movement and positioning in response to an external magnetic field and easy separation of the samples from the surrounding medium, which are crucial for targeted drug delivery applications.[34–42]

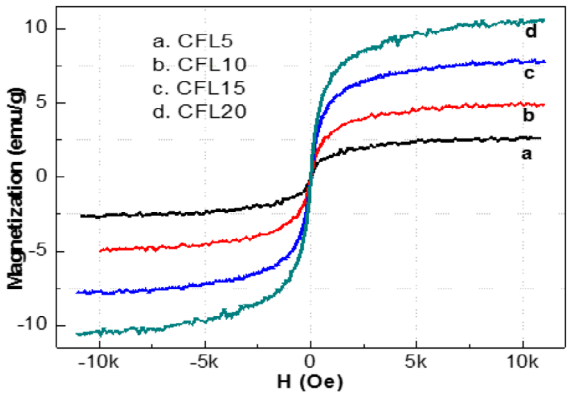

Figure 3. Magnetic saturation curves of CFL5, CFL10, CFL15, and CFL20.

3.2. Morphology of CFL Films

FE-SEM images of Fe_3O_4, pure Lov and the composite films are shown in Figure 4. It can be seen that the Fe_3O_4 particle is about 15-17 nm and the pure Lov particles were bar-shaped crystals with size from 10 μm–40 μm. When incorporated in the CFL films, Lov particles became spherical and well dispersed into the CS matrix due to the hydrogen bonds formed between CS and Lov. Without Fe_3O_4 doping, the **CFL0** film exhibited a more uniform dispersion of spherical Lov particles resulting in less agglomeration. When adding Fe_3O_4 nanoparticles at different concentrations to the CS matrix, large spherical Lov particles tended to clump together to form larger clusters and concentrate on the CS surface. This could be explained by the fact that Fe_3O_4 nanoparticles dispersed into CS also formed hydrogen bonds with CS, affecting the ability to form initial hydrogen bonds between Lov and CS, thereby also affecting the solubility of Lov in buffer solutions.

3.3. Distribution of Elements in CFL Films

The spatial distribution of elements in the composite films was investigated by EDX method and the results obtained for sample **CFL0**, **CFL10,** and **CFL20** were shown in Figure 5. It can be seen from the element maps that the C (red) and O (green) elements were found as major elements in all samples while the Fe (yellow) element was only present in samples **CFL10** and **CFL20**. Additionally, it is evident that the yellow color in samples **CFL10** and **CFL20** is unevenly distributed, which is consistent with FE-SEM results showing that Fe_3O_4 nanoparticles were agglomerated and thus unevenly distributed into the CS matrix. The results in Figure 4 and 5 showed that lovastatin was well dispersed within the chitosan matrix, with particle sizes ranging from 10 to 40 μm, and they distributed in matrix of Fe_3O_4 nanoparticles.

3.4. X-ray Diffraction (XRD) Analysis

Figure 6 shows the X-ray diffraction (XRD) spectra of three samples: pure lovastatin, Fe_3O_4 nanoparticles, and CFL10 composite

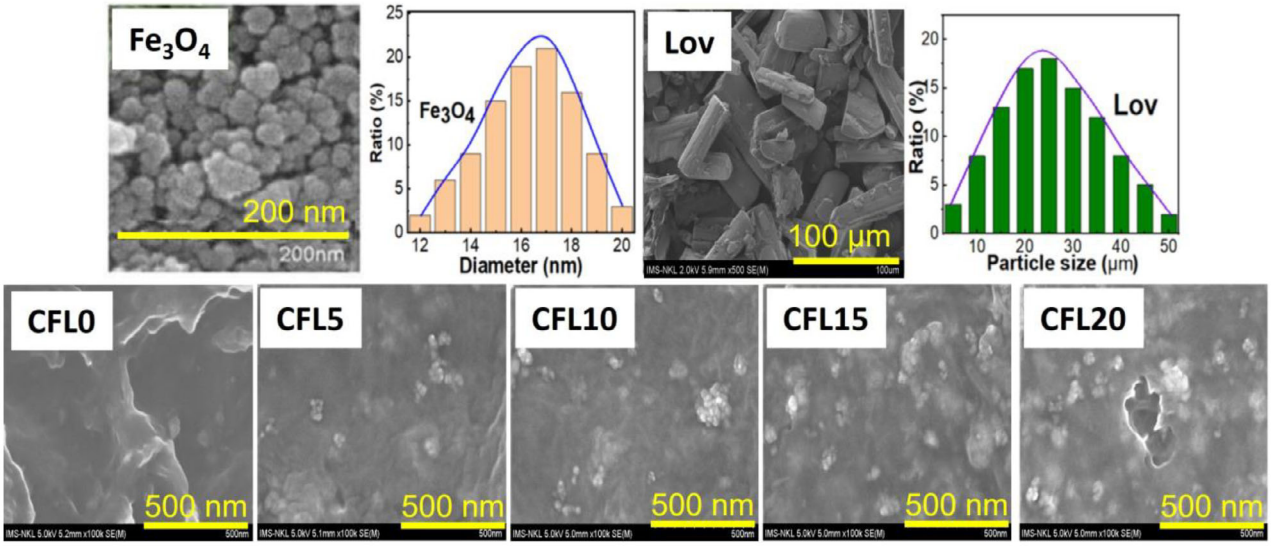

Figure 4. FE-SEM images of Fe_3O_4, Lov, and CFL films with various Fe_3O_4 concentrations (0%– 20%).

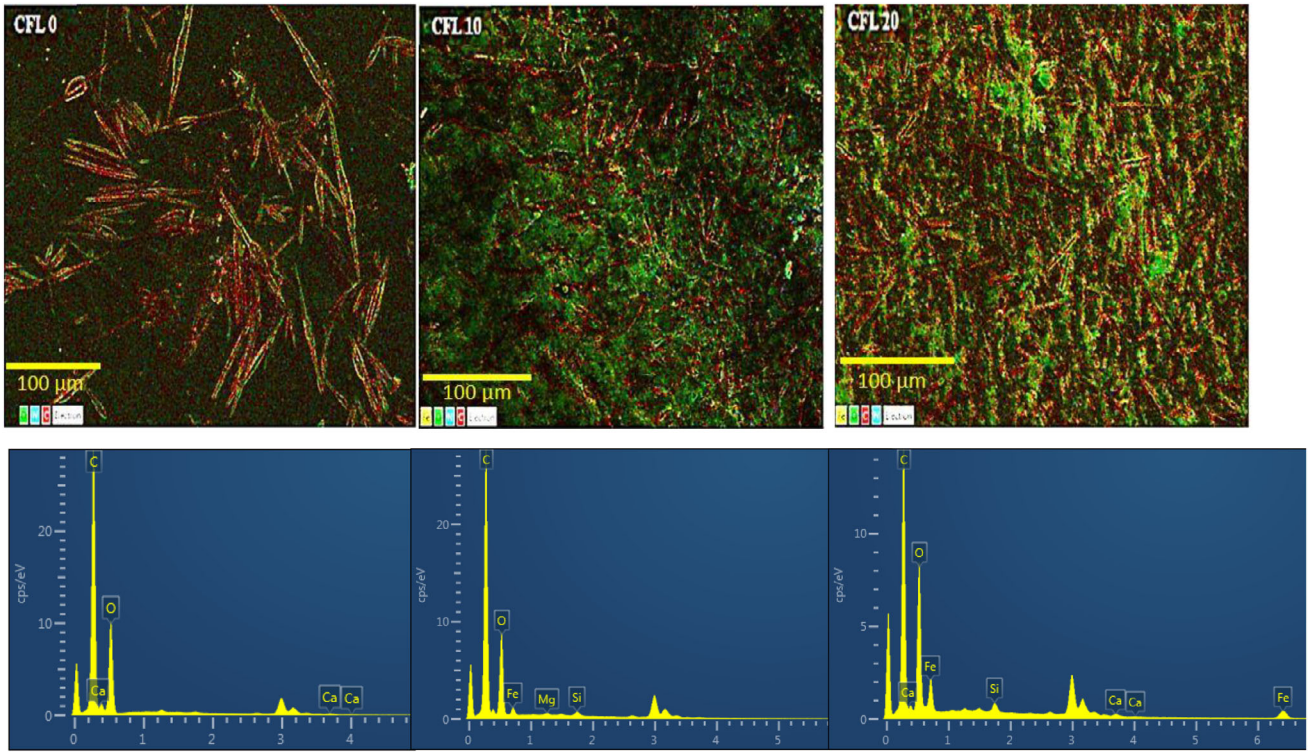

Figure 5. EDX and element maps of **CFL0**, **CFL10,** and **CFL20**: C (red), O (green), Fe (yellow).

film. The XRD spectrum of Lov exhibits many sharp peaks mainly in the 2θ region from 10 to 30°, which is characteristic of the crystalline nature of Lov. This result is consistent with the study of Mahmood et al. (2019).[47] Meanwhile, the Fe_3O_4 particle sample exhibits sharp diffraction peaks at 2θ positions approximately 30.1°, 35.5°, 43.1°, 53.4°, 57.0°, and 62.6°, corresponding to the (220), (311), (400), (422), (511), and (440) planes of the cubic spinel structure of magnetite. These peaks are in good agreement with the previous report by Bertolucci.[48] Notably, the diffraction spectrum of sample CFL10 showed a sharp decrease in intensity and peak broadening, especially at the peak positions of Lov and Fe_3O_4. The characteristic peaks of Fe_3O_4 were still present but were fainter, indicating that the nanoparticles were well dispersed in the CS matrix and were surrounded by the polymer network. At the same time, the disappearance of the diffraction peaks of Lov indicated that the drug had changed from a crystalline state to an amorphous or semi-amorphous state when dispersed into the polymer matrix. In this phenomenon, interactions such as hydrogen bonding and electrostatic interactions between the drug and the polysaccharide chain disrupted

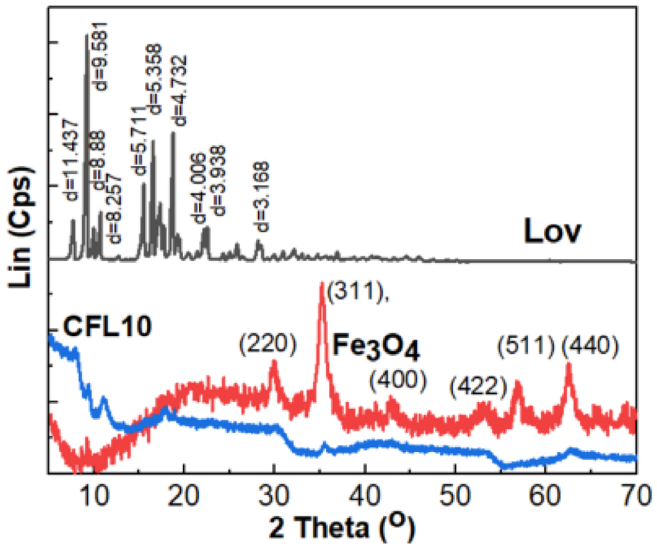

Figure 6. XRD spectra of Lov, Fe_3O_4, and CFL10 composite membranes.

the original crystalline order. Similar material systems using chitosan or carrageenan have been reported previously with similar diffraction characteristics.[49] This change in the structural state may be beneficial in terms of applicability, since amorphous drugs often have a faster dissolution rate.

3.5. Thermogravimetric Analysis (TGA) of CFL Film

Thermogravimetric (TG) and differential thermal (dTG) analysis were performed to evaluate the thermal properties and compositional stability of the composite samples. Figure 7 shows the TG and dTG spectra of CFL0 and CFL10 samples, in air from room temperature to 800 °C at a heating rate of 10 °C/min. The TG spectrum of CFL10 sample shows three main stages of mass loss. The first decomposition stage occurred at approximately 97.4 °C, corresponding to 15.5% of the mass loss, which is attributed to the evaporation of free water and physically bound water in the chitosan structure. This phenomenon is consistent with hydrophilic polysaccharides such as chitosan, which usually lose their initial mass below 120 °C due to moisture release.[50] The second degradation stage, recorded at 304.4 °C, accounted for 35.7% of the mass loss and reflected the main degradation processes of the chitosan backbone, including polymer degradation, deacetylation, and glycosidic bond cleavage. Thermal degradation of lovastatin was also expected to occur in this range, as previous studies reported the drug to decompose in the range of 280–320 °C.[51] The third and largest mass loss stage occurred at approximately 426.9 °C, resulting in a further 43.4% mass loss. This stage involved oxidative combustion of the carbon residue and complete decomposition of the remaining organic components. The total mass loss amounted to approximately 94.6%, leaving a residue of approximately 5.4%, which corresponds well to the theoretical Fe_3O_4 content (10% by mass relative to chitosan). The high thermal stability of Fe_3O_4 under oxidizing conditions up to 700–800 °C supports this conclusion.[52]

Compared with the chitosan/lovastatin system (CFL0), which does not leave significant residue after 700 °C, the presence of Fe_3O_4 in CFL10 significantly enhanced the thermal stability at the final degradation stage. This suggests a synergistic interaction between the inorganic filler and the polymer–drug system, possibly through thermal shielding, catalysis, or hydrogen bonding mechanisms. These results not only confirm the successful dispersion of Fe_3O_4 in the composite structure, but also highlight the potential application of the material in improving the thermal stability of biobased drug delivery systems.

3.6. Thermal Properties Analysis by DSC

The chitosan sample exhibited a sharp endothermic peak at ~59.8 °C, corresponding to the dehydration process due to the evaporation of weakly bound water in the polymer network. In addition, a mild exothermal peak could be observed in the 150–200 °C region, reflecting the onset of polymer chain degradation. These characteristics are consistent with previous reports, which showed that chitosan typically has a dehydration region in the range of 50–80 °C, in addition to the sample starting to decompose at around 280–320 °C.[54] Pure lovastatin showed a clear melting peak at ~174.6 °C, which is characteristic of the crystalline structure of the active substance[55] and indicating that the sample is thermally stable and has not undergone any physicochemical changes.

The DSC curve of the CFL0 sample exhibited an endothermic peak at 46.8 °C with an absorption energy value of 450.5 J/g. This peak was shifted lower than that of pure chitosan (~59.8 °C), indicating that the interaction between chitosan and lovastatin occurred, which weakened the internal hydrogen network of chitosan, thereby reducing the dehydration temperature. At the same time, no clear melting peak of lovastatin was observed at 174 °C, suggesting that lovastatin was molecularly dispersed or non-crystalline incorporated in the polymer matrix.[56] When 10% Fe_3O_4 nanoparticles were added, the CFL10 sample exhibited a shift of the endothermic peak to ~55–60 °C and the height and area of the endothermic peak decreased slightly compared to CFL0. The increase in this temperature indicates improved thermal stability of the composite, which may be a result of interactions between the functional groups $–NH_2$, –OH of chitosan and the Fe_3O_4 surface through hydrogen bonding or ionic interactions. This interaction stiffens the polymer network structure, increasing the energy required to dehydrate or break the intra-network interactions.[57] The disappearance of the melting peak of lovastatin in both CFL0 and CFL10 samples further confirms that lovastatin has transformed into an amorphous state or is strongly bound to the chitosan matrix, which is important for improving the biosolubility of the drug. Thus, the CFL10 sample shows improved thermal properties indicating the dispersibility and film-forming ability of chitosan as well as the structural stabilization ability of Fe_3O_4. This suggests that the CFL10 material system is a potential candidate for drug delivery applications that require high stability and good drug dispersion.

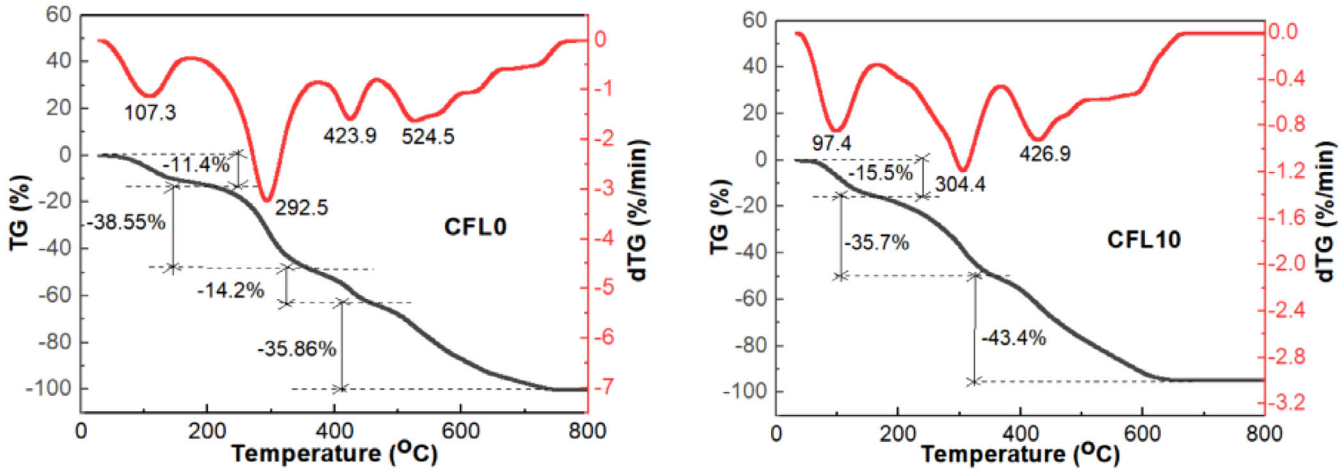

Figure 7. TG/DTG spectra of CFL0 and CFL10 composite films.

3.7. Effect of Fe_3O_4 Content on the Mechanical Properties of CFL Composite Films

Mechanical properties are essential factors in evaluating the applicability of biopolymer films in drug delivery, especially in controlled drug release systems. In this study, CFL composite film samples with Fe_3O_4 nanoparticle ratios varying from 0% to 20% (compared to chitosan mass) were investigated for tensile properties. The main mechanical parameters included elastic modulus (E-modulus), ultimate stress (Rm), elongation at break (ε-bruch) and stress at maximum force (RB). The sample without particles (CSL0) had the highest elastic modulus (1369.53 MPa), tensile stress of 43.18 MPa and ε-bruch of only 7.94%, reflecting the stiff but less flexible mechanical properties typical of pure chitosan films. When 5% Fe_3O_4 was added (sample CFL5), the material tended to be softer ($E = 791.78$ MPa), but at the same time reached the highest Rm value in the series (52.82 MPa) and ε-bruch increased nearly twice (15.38%) compared to the control sample, indicating the enhancement effect in both tensile strength and ductility due to the proper dispersion of Fe_3O_4 nanoparticles. A clear change was observed in sample CFL10 (10% Fe_3O_4), with ε-bruch and ε-F max exceeding 58%, while the elastic modulus decreased sharply to 309.68 MPa. This shows that at this concentration, the material system becomes extremely flexible, suitable for applications requiring high elasticity. However, the tensile stress Rm tended to decrease (41.93 MPa), reflecting the trade-off between ductility and strength – a common phenomenon in hybrid inorganic polymer systems containing a filler ratio sufficient to soften the polymer network but not sufficient to cause agglomeration. For samples containing between 15% and 20% Fe_3O_4 (CFL15 and CFL20), the elastic modulus increased again (1090.30 and 1159.22 MPa, respectively), indicating a return of stiffness. However, the elongation at break decreased sharply (14.81% and 7.38%) along with a decrease in Rm values to 31.51 and 30.56 MPa. This is explained by the agglomeration of Fe_3O_4 particles at high concentrations, creating micro-defects in the material structure and causing stress concentration, thereby leading to premature failure under tensile stress. Thus, the results showed that the Fe_3O_4 ratio of 5%–10% is optimal to simultaneously improve the strength and ductility of the material. Low ratios increase elongation and effective force distribution, while high ratios cause embrittlement. In addition, Rinaudo (2006) also confirmed that chitosan tends to become more brittle when containing too much inorganic filler phase, due to the decrease in hydrogen bonding and reduced deformability of the polymer network.[50]

Table 3. Cell viability inhibition (%) and IC_{50} values for the tested composite samples on Vero cells.

Sample Code	Cell Inhibition (%)	IC_{50} (μg/mL)
Negative Control	0.00	–
Positive Control	93.04 ± 1.12	0.32
CFL0	5.65 ± 0.13	>128
CFL10	27.81 ± 0.34	>128

3.8. Cytotoxicity Evaluation Using the MTT Assay

The MTT assay was used to evaluate the cell proliferation inhibition ability of the composite materials on the normal Vero cell line. The results presented in Table 3 show that both tested samples CFL0 and CFL15 were not toxic to the Vero cell line at concentrations up to 128 μg/mL, with inhibition rates between 5.65 ± 0.13% and 27.81 ± 0.34%, respectively and IC_{50} values were both greater than 128 μg/mL. The cell proliferation inhibition levels of both samples were lower than the biological activity threshold (≥ 50%), indicating that these material systems were safe for normal cells under in vitro conditions. In particular, the CFL15 sample, although containing high Fe_3O_4 magnetic nanoparticles, still maintained high biocompatibility, demonstrating that the integration of Fe_3O_4 into the chitosan matrix does not cause additional toxicity but can create a biologically safer drug delivery system. This result is consistent with previous studies showing that chitosan is a safe biopolymer and Fe_3O_4 is widely used in drug delivery and biomedical imaging.[52]

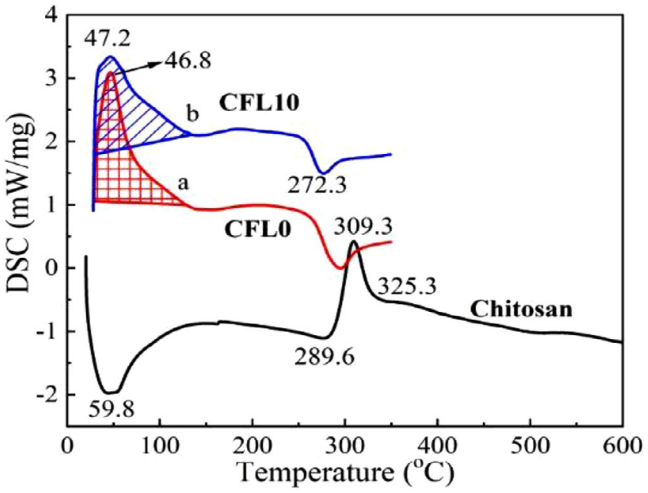

Figure 8. Water absorption of CFL membrane.

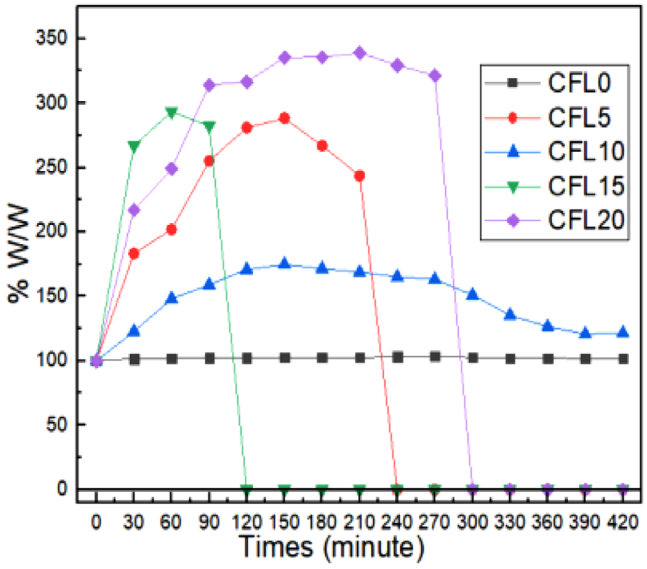

Figure 9. Lov release from the CFL films in pH 2.0 environment at 37 °C.

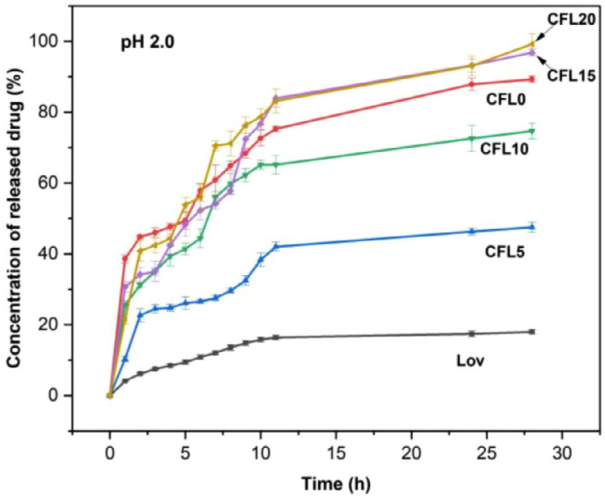

Figure 10. Lov release from the CFL films in pH 7.4 environment at 37 °C.

Compared with the positive standard (e.g., ellipticine or paclitaxel), the cell inhibition rate was above 90%, and the IC_{50} value was only 0.32 μg/mL, further emphasizing the safety of the CFL samples under the test conditions.

3.9. Long-Term Swelling Behavior of CFL Films

The ability to swell over time is an important indicator reflecting the stability and structural strength of biofilm materials in a humid environment. CFL samples with varying Fe_3O_4 content, after 30–120 min, the samples containing Fe_3O_4 all showed a significant increase in mass, with the swelling peak reaching at 120 min for samples CFL5 (280.98%), CFL10 (170.88%), CFL15 (293.58%) and CFL20 (316.67%), respectively (Figure 8). In particular, sample CFL0 (without Fe_3O_4) remained almost constant throughout 420 min (ranging from ~101.9%–103.9%), indicating that the Cs/Lov polymer network is not able to absorb water effectively without the inorganic phase. After 120 min, the swelling level of the samples began to change in the direction of decomposition. The CFL15 sample rapidly decreased to 0% from 150 min and remained at 0% until the end of the test cycle, indicating that the membrane structure was completely destroyed after excessive swelling. The CFL5 sample began to decrease rapidly from 180 min and completely lost its ability to swell from 240 min onwards. The CFL20 sample had the highest and most stable swelling until 240 min (329.47%), then began to decrease and also fell to 0% from 300 min onwards. Although the CFL10 sample had a lower swelling, it remained relatively stable until the end of the test (121.6% at 420 min), indicating that its structural stability was much better than the other samples. Thus, considering both performance and durability, sample CFL10 was considered the most optimal in the series of investigations: although it did not reach the maximum swelling, it still maintained over 120% after 7 h, while samples with higher swelling (CFL15, CFL20) suffered network breakdown and fell to 0% after 5 h of immersion. Samples CFL15 and CFL5 were considered poor because they could not maintain stable swelling beyond 240 min. The early loss of swelling ability may be related to excessive swelling leading to cracking or physical disintegration of the polymer network.[53] The Fe_3O_4 content also significantly affected both water absorption performance and structural durability and optimizing the content at a medium level (10%) could provide a balance between swelling ability and morphological stability in drug delivery or soft tissue materials applications.

3.10. In Vitro Release of Lov from CFL Composite Films with Various Fe_3O_4 Content in Different pH Buffers

The results obtained when monitoring the release of Lov from itself and from the composite films over time in pH 2.0 and 7.4 buffer solutions at 37 °C are presented in Figures 9 and 10. Overall, the curves exhibit a fairly rapid release of Lov during the first

Table 4. Percentage of Lov released at pH 2.0 and pH 7.4 after 28 h of testing.

Sample	Lov	CFL0	CFL5	CFL10	CFL15	CFL20
pH 2.0	17.97%	89.28%	47.45%	74.67%	96.8%	99.2%
pH 7.4	30.86%	87.24%	91.13%	97.12%	51.12%	98.9%

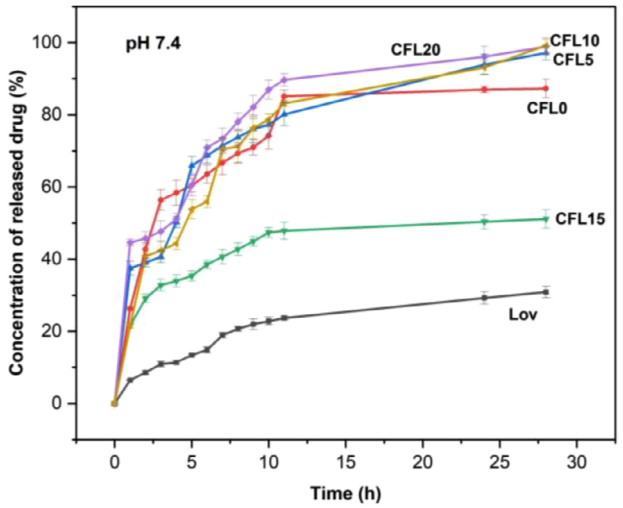

Figure 11. DSC diagram of CFL0 and CFL10 composite membranes.

10 h of testing, followed by a slower release period. The results reveal a clear influence of the CS matrix and the Fe_3O_4 addition on the ability to release Lov in both simulated solutions. For clarity, the percentages of Lov released after 28 hours are shown in Table 4 and Figure 9.

When not incorporated into the polymer matrix, the release ability of free Lov particles could only reach between 17.97% and 30.86% at pH 2.0 and 7.4, respectively, after 28 h of testing (sample **Lov**). Meanwhile, when loaded on the CS matrix, the release ability of Lov increased (sample **CFL0**) because the small-sized Lov particles were well dispersed into CS and released gradually. Alternatively, Lov release also occurred with the dissolution of CS into the solution causing them to disintegrate into smaller Lov-carrying fragments; Lov was then released from these clumps into the solution. Therefore, the percentage of Lov released after 28 h increased sharply to 89.29% and 87.24% at pH between 2.0 and 7.4, respectively.

It can be seen from Figure 11 that the ability to release Lov also varied with the Fe_3O_4 concentration in the CS films. At pH 2.0, the CS films doped with Fe_3O_4 between 5% and 10% exhibited a decrease in the ability to release Lov while the CS films with 15% and 20% of Fe_3O_4 showed an increased release of Lov compared to the CS film. This could be because, at small concentrations, Fe_3O_4 nanoparticles were better dispersed into the CS matrix, making the CS structure more stable, thus reducing the ability of CS films to dissolve, leading to a slower release of Lov. In Figure 12, at higher Fe_3O_4 doping concentrations (15% and 20%), Fe_3O_4 nanoparticles tended to aggregate locally to form clusters. These clusters were then dissolved in the acidic solution (pH 2.0), causing a decrease in the mechanical strength of the CS films and the bonding strength between CS and Lov. As a result, the CS films became easier to disintegrate, and thus Lov was released more easily. The amount of Lov released from the samples **CFL5**, **CFL10**, **CFL15**, and **CFL20** after 28 h were 47.45%, 74.67%, 96.8%, and 99.2%, respectively, compared to 89.28% released in the sample **CFL0**.

In contrast, in a neutral medium (pH 7.4), the release behavior of Lov from the CFL films appears to be simpler (except for **CFL15**) with a slight increase in the amount of Lov released when increasing the Fe_3O_4 concentration. This may be because the hydrogen bonds between CS and Lov were broken at higher pH, causing Lov to release more easily. This result was also consistent with other studies.[41,42,46] After 28 h of testing, the Lov amounts released from **CFL5**, **CFL10**, **CFL15**, and **CFL20** were 91.13%, 97.12%, 51.12%, and 98.9%, respectively. Therefore, sample **CFL10** was suitable for use as a Lov release model because the Fe_3O_4 ratio was not too high (10%) but still achieved good Lov release efficiency in simulated body fluids.

Table 5 and Figure 9 also showed that Lov was released more rapidly in the neutral medium than in the acidic medium. The acidic environment can cause repulsion between H^+ ions and cations on the surface of CS, which inhibits polymer hydrolysis.[42–44,46] The results in Table 5 show that the amount of Lov released is significantly higher at pH 7.4 than in the work.[44] These results at Table 5 were also consistent with the work of Thai Hoang et al. on the release ability of Lov from alginate/chitosan-based composites at different pH values (pH: 2.0; 4.5; 6.5; and 7.4).[45] However, high Fe_3O_4 doping concentrations led to the opposite trend, as explained above. Moreover, in this study, to increase the biocompatibility of Fe_3O_4 nanoparticles, they were dispersed in a PEG solution before incorporating into the CS matrix.[45] This may also explain the better control of drug release of the composite films in the presence of Fe_3O_4 nanoparticles.

However, at high Fe_3O_4 doping levels, an exception was observed. Specifically, the release percentage decreased at CFL15 but increased again at CFL20. This biphasic trend may be attributed to the complex effect of Fe_3O_4 on the structural integrity of the composite matrix. At 15% Fe_3O_4 loading, excessive nanoparticle content likely causes aggregation within the CS network, obstructing diffusion pathways and reducing Lov mobility, thereby leading to a lower release rate. In contrast, at 20% Fe_3O_4, the high degree of aggregation and local accumulation may disrupt the CS structure, increasing porosity or forming micro-fractures that facilitate drug release. Similar nonlinear trends have been reported in nanoparticle-polymer systems where moderate doping reinforces the matrix, but excessive loading compromises its integrity.

Moreover, in this study, to improve the biocompatibility of Fe_3O_4 nanoparticles, they were pre-dispersed in a PEG solution before being incorporated into the CS matrix.[45] This approach likely contributed to better control of the release profile by improving the dispersion of Fe_3O_4 and modulating the interaction with the polymer network.

From these findings, it can be concluded that the CFL films are more suitable for drug delivery in the environments of the large intestine, colon, and rectal mucosa rather than

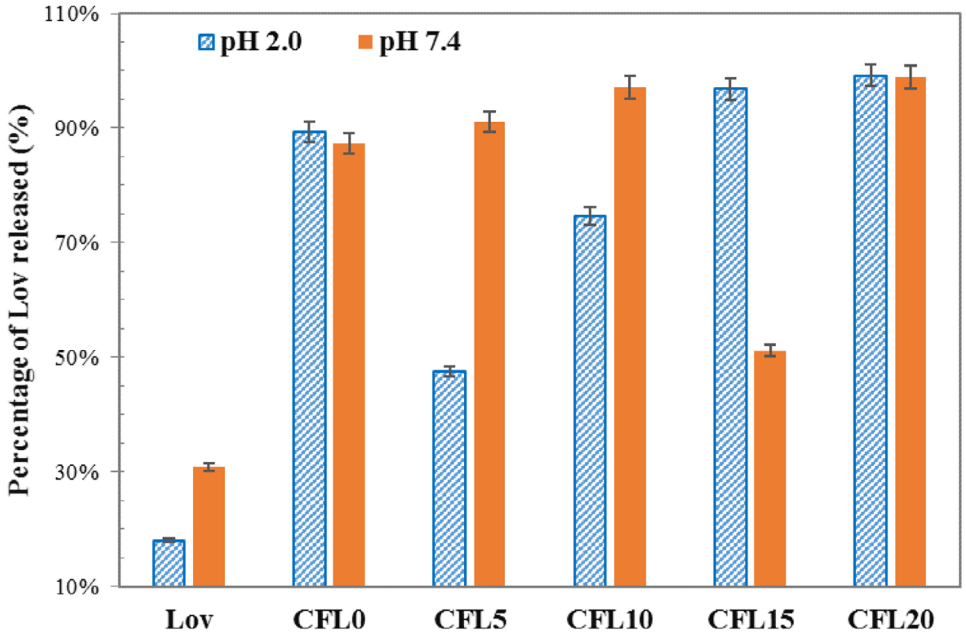

Figure 12. Percentage of Lov released at pH 2.0 and 7.4 after 28 h of testing.

Table 5. Mechanical properties of CFL films with varying Fe_3O_4 content.

Sample	E-Modul (MPa)	ε-F max (%)	RB (MPa)	ε-Bruch (%)	Rm (MPa)
CSL0	1369.53	7.53	42.84	7.94	43.18
CFL5	791.78	14.46	51.21	15.38	52.82
CFL10	309.68	58.71	41.16	58.79	41.93
CFL15	1090.30	12.73	26.09	14.81	31.51
CFL20	1159.22	4.14	26.55	7.38	30.56

the acidic gastric fluid. Furthermore, the optimal Fe_3O_4 doping concentration should be maintained below 15% to avoid undesirable aggregation and structural disruption that may lead to inconsistent release behavior.

3.11. Kinetics of Lov Release from CFL Composite Films with Various Fe_3O_4 Content in Different pH Buffers

The kinetics of Lov release from the CFL composite films in solutions between pH 2.0 and 7.4 were studied based on the models of zero-order kinetics (ZO), first-order kinetics (FO), Higuchi (HG), the Hixson-Crowell (HCW), and the Korsmeyer-Peppas (KMP). Based on the regression coefficient, the most suitable release mechanism and kinetic model for Lov release could be determined. The model with the largest regression coefficient (closer to 1) was the most appropriate. The kinetic parameters obtained with different models are given in Table 6.

Among the tested models, Higuchi and Korsmeyer–Peppas provided the best fit to the experimental data, with R^2 values ranging from 0.899 to 0.985 across most samples, indicating that drug release was predominantly governed by diffusion through the polymer matrix. The zero-order model also demonstrated a relatively good fit, particularly in acidic medium (pH 2.0), with the highest R^2 values observed for CFL0 (0.982) and CFL15 (0.965), suggesting a near-constant release rate under these conditions. In contrast, the first-order model showed the lowest correlation, especially at pH 7.4 (e.g., $R^2 = 0.754$ for CFL0), indicating that the release rate was not directly proportional to the remaining drug content in the matrix. The release exponent n values obtained from the KMP model ranged from 0.128 to 0.386, which are characteristic of Fickian diffusion-controlled release mechanisms ($n < 0.45$) for all samples. Notably, an increasing trend in n was observed with higher Fe_3O_4 content, particularly at pH 7.4, where n increased from 0.304 (CFL0) to 0.376 (CFL20). This suggests a possible transition toward anomalous (non-Fickian) transport, where both diffusion and polymer matrix relaxation contribute to the release mechanism.

Overall, the release kinetics were strongly influenced by the pH of the medium. Higher R^2 values in acidic conditions imply that the drug delivery system performs more efficiently in simulated gastric environments, making it a promising candidate for stomach-targeted drug delivery applications.

4. Conclusion

Chitosan-based composite films doped with varying concentrations of Fe_3O_4 nanoparticles were synthesized and evaluated as a lovastatin delivery system in simulated body fluids. The components in these films are good compatibility. The addition of Fe_3O_4 nanoparticles to the composite films affect strongly on the morphology, crystal structure, thermal stability, swelling capacity and mechanical properties of these films. The composite films did not cause the toxicity on the Vero cells.

The incorporation of Fe_3O_4 nanoparticles (0%–20% w/w relative to chitosan) resulted in superparamagnetic behavior with

Table 6. Regression equation parameters obtained with different models and the release information of Lov from the CFL films in pH 2 and pH 7.4 solutions.

		CFL0		CFL5		CFL10		CFL15		CFL20	
		pH 2.0	pH 7.4	pH 2.0	pH 7.4	pH 2.0	pH 7.4	pH 2.0	pH 7.4	pH 2.0	pH 7.4
ZO	R^2	0.982	0.869	0.859	0.854	0.970	0.904	0.965	0.956	0.954	0.972
FO	R^2	0.955	0.754	0.783	0.893	0.928	0.784	0.973	0.811	0.813	0.926
HG	R^2	0.946	0.928	0.862	0.935	0.958	0.929	0.906	0.985	0.968	0.972
HCW	R^2	0.982	0.795	0.791	0.955	0.963	0.884	0.982	0.918	0.902	0.965
KMP	R^2	0.904	0.934	0.861	0.936	0.950	0.899	0.886	0.964	0.961	0.877
	n	0.355	0.304	0.128	0.386	0.232	0.325	0.256	0.222	0.235	0.376

saturation magnetization values ranging from 2.6 to 10.8 emu/g in a magnetic field H of 10,000 Oe. The CFL films showed a good ability to release Lov at pH 2.0 and 7.4 compared to the free drug. The study also indicated the influence of nano-Fe_3O_4 on the ability to release Lov drug from the composite films at pH 2.0 and 7.4. At pH 2.0, Fe_3O_4 nanoparticles inhibited the Lov release, while at pH 7.4, they increased the Lov release compared to the sample without Fe_3O_4 because they affected the stability of CFL composite films. After 28 hours at pH 2.0, the samples **CFL5**, **CFL10**, **CFL15**, and CFL20 released 47.45%, 74.67%, 96.8%, and 99.2% of their total Lov, while the sample **CFL0** released 89.28%. Following 28 hours of testing, the Lov quantities released from **CFL5**, **CFL10**, **CFL15**, and **CFL20** were 91.13%, 97.12%, 51.12%, and 98.9%, respectively, in a neutral medium (pH 7.4). All of the composite films' drug release kinetic characteristics were regulated by Fickian diffusion and better matched the Korsmeyer-Peppas model. The drug release kinetic behaviors from all the composite films were better fitted to the Korsmeyer-Peppas model and were controlled by Fickian diffusion. These results suggest that the nano-Fe_3O_4 doping concentration should be less than 15% and that the CFL films are better suited to the environment of the large intestine, colon, and rectal mucosa than the acidic environment of gastric juice. In particular, sample **CFL10** was appropriate for use as a Lov release model since it demonstrated good Lov release efficiency in simulated bodily fluids while having a Fe_3O_4 ratio that was not excessively high (10%).

Acknowledgment

The authors have nothing to report.

Conflict of Interests

The authors declare no conflict of interest.

Author Contributions

V.Q.M., T.M.T., and **D.T.Y.**: Investigation, methodology, formal analysis. **N.T.H.N., L.N.L.,** and **N.T.B.V.**: Investigation. **H.M.H., N.N.L., N.T.B.V.,** and **V.T.H.**: Validation. **H.T.,** and **N.T.C.**: Writing—reviewing and editing, supervision. **V.Q.T.**: Investigation, conceptualization, writing—original draft preparation, payment for chemicals, and measurements.

Data Availability Statement

The data that support the findings of this study are available from the corresponding author upon reasonable request.

Keywords: Chitosan film · Drug release · Evaporation casting method · Fe_3O_4 nanoparticles · Lovastatin

[1] S. Rahmati-Ahmadabad, D. R. Broom, A. Ghanbari-Niaki, H. Shirvani, *Life Sci.* **2019**, *224*, 139-148, https://doi.org/10.1016/j.lfs.2019.03.058.
[2] J. Plat, S. Baumgartner, T. Vanmierlo, D. Lütjohann, K. L. Calkins, D. G. Burrin, G. Guthrie, C. Thijs, A. A. T. Velde, A. C. E. Vreugdenhil, R. Sverdlov, J. Garssen, K. Wouters, E. A. Trautwein, T. G. Wolfs, C. Gorp, M. T. Mulder, N. P. Riksen, A. K. Groen, R. P. Mensink, *Prog. Lipid Res.* **2019**, *74*, 87-102, https://doi.org/10.1016/j.plipres.2019.02.003.
[3] A. Alloubani, R. Nimer, R. Samara, *Curr. Cardiol. Rev.*, **2021**, *17*, e051121189015.
[4] D. S. Gesto, C. M. S. Pereira, N. M. F. S. Cerqueira, S. F. Sousa, *Molecules* **2020**, *25*, 3891, https://doi.org/10.3390/molecules25173891.
[5] N. Ferri, M. Ruscica, S. Fazio, A. Corsini, *J. Clin. Med.* **2024**, *13*, 943, https://doi.org/10.3390/jcm13040943.
[6] M. J. Qureshi, C. Mallikarjun, W. G. Kian, *Asian J. Pharm. Sci.* **2015**, *10*, 40.
[7] N. Zolkiflee, M. M. M. Affandi, A. Majeed, *Int. J. Res. Pharm. Sci.* **2017**, *8*, 90.
[8] J. Zhou D. Zhou, *Drug Des. Devel. Ther.* **2015**, *5269*, 26425076.
[9] Q. Guan, W. Chen, X. Hu, *Drug Des. Devel. Ther.* **2015**, *791*, 25709403.
[10] G. Satchanska, S. Davidova, P. D. Petrov, *Polymers*, **2024**, *16*, 1159.
[11] A. Cansel Tiryaki, O. Vardar, Y. Yildirim, A. Nalbantsoy, N. B. Sarikahya, *ChemistrySelect* **2023**, *8*, e202302658, https://doi.org/10.1002/slct.202302658.
[12] H. Thai, D. L. Tran, T. L. Thach, D. G. Le, M. T. D. Tran, Q. T. Vu, T. A. Nguyen, D. T. Nguyen, T. C. Nguyen, *J. Polym. Environ.* **2019**, *27*, 2728-2738, https://doi.org/10.1007/s10924-019-01550-8.
[13] K. S. Phan, T. T. H. Le, T. M. Nguyen, T. T. T. Mai, P. H. Hoang, X. T. To, T. T. Nguyen, K. D. Pham, P. T. Ha, *ChemistrySelect*, **2022**, *7*, e202201954.
[14] L. S. Ganapathe, M. A. Mohamed, R. Mohamad Yunus, D. D. Berhanuddin, *Magnetochemistry* **2020**, *6*, 68.
[15] T. M. Thi, V. Q. Trung, D. K. Tung, P. T. Thanh, N. H. Yen, N. M. Lam, *Jpn. J. Appl. Phys.* **2021**, *60*, 025001, https://doi.org/10.35848/1347-4065/abd86d.
[16] Shima, P. Damodaran, *ChemistrySelect* **2020**, *5*, 9261-9268, https://doi.org/10.1002/slct.202001102.
[17] M. D. Nguyen, H.-V. Tran, S. Xu, T. R. Lee, *Appl. Sci.* **2021**, *11*, 11301, https://doi.org/10.3390/app112311301.

[18] B. A. Eldeeb, W. M. A. El-Raheem, S. Elbeltagi, *Sci. Rep.* **2023**, *13*, 19000, https://doi.org/10.1038/s41598-023-46287-6.
[19] G. Kasparis, A. P. Sangnier, L. Wang, C. Efstathiou, A. P. LaGrow, A. Sergides, C. Wilhelm, T. K. T. Nguyen, *J. Mater. Chem. B* **2023**, *11*, 787-801, https://doi.org/10.1039/D2TB01338J.
[20] M. Kamalzare, M. R. Ahghari, M. Bayat, A. Maleki, *Sci. Rep.* **2021**, *11*, 20021, https://doi.org/10.1038/s41598-021-99121-2.
[21] M. Sakaguchi, M. Makino, T. Ohura, K. Yamamoto, Y. Enomoto, H. Takase, *Adv. Powder Technol.* **2019**, *30*, 795-806, https://doi.org/10.1016/j.apt.2019.01.008.
[22] H. V. T. Luong, M. T. Diep, N. Y. Nguyen, D. T. Pham, L. N. H. Cao, T. M. P. Ha, *J. Drug Deliv. Sci. Technol.* **2024**, *93*, 105465, https://doi.org/10.1016/j.jddst.2024.105465.
[23] M. S. Jabir, U. M. Nayef, W. K. A. Kadhim, *Nano Biomed. Eng.*, **2019**, *11*, 18.
[24] N. D. Arnold, W. M. Brück, D. Garbe, T. B. Brück, *Mar. Drugs* **2020**, *18*, 93, https://doi.org/10.3390/md18020093.
[25] G. Unsoy, U. Gunduz, *Nano. Dru. Deli.*, Vol. *835*, Elsevier, Saint Louis **2017**, https://doi.org/10.1016/b978-0-323-46143-6.0026-9.
[26] D. Wang, J. Li, H. Li, F. Tang, *Trans. Nonferrous Met. Soc. China* **2009**, *19*, 1232-1236, https://doi.org/10.1016/S1003-6326(08)60434-3.
[27] Z. Wang, Q. Ye, S. Yu, B. Akhavan, *Adv. Healthcare Mater.* **2023**, *12*, 2300105, https://doi.org/10.1002/adhm.202300105.
[28] A. A. D'souza, R. Shegokar, *Expert Opin. Drug Deliv.* **2016**, *13*, 1257.
[29] A. Bunker, *Phys. Procedia* **2012**, *34*, 24.
[30] C.-H. Chen, J.-C. Yang, Y.-S. Uang, C.-J. Lin, *Int. J. Pharm.* **2013**, *444*, 18-24, https://doi.org/10.1016/j.ijpharm.2013.01.028.
[31] S. Beg, P. S. Sandhu, R. S. Batra, R. K. Khurana, B. Singh, *Drug Deliv* **2015**, *22*, 765-784, https://doi.org/10.3109/10717544.2014.900154.
[32] Y. Zhang, H. Zhang, E. Che, L. Zhang, J. Han, Y. Yang, S. Wang, M. Zhang, C. Gao, *Colloids Surfaces B: Biointerfaces* **2015**, *128*, 77-85, https://doi.org/10.1016/j.colsurfb.2015.02.021.
[33] K. C. L. Mulder, F. Mulinari, O. L. Franco, M. S. F. Soares, B. S. Magalhães, N. S. Parachin, *Biotechnol. Adv.* **2015**, *33*, 648-665, https://doi.org/10.1016/j.biotechadv.2015.04.001.
[34] A. Drabczyk, S. Kudłacik-Kramarczyk, M. Głąb, M. Kędzierska, A. Jaromin, D. Mierzwiński, B. Tyliszczak, *Materials* **2020**, *13*, 3073, https://doi.org/10.3390/ma13143073.
[35] R. Dikshit, P. Tallapragada, *J. Food Drug Anal.* **2016**, *24*, 433.
[36] A. A. Gadgeel, S. T. Mhaske, C. Duerr, K. L. Liu, *J. Inorg. Organomet. Polym. Mater.* **2019**, *29*, 1688-1700, https://doi.org/10.1007/s10904-019-01131-1.
[37] G. Antarnusa, P. D. Jayanti, Y. R. Denny, A. Suherman, *Materialia* **2022**, *25*, 101525, https://doi.org/10.1016/j.mtla.2022.101525.
[38] A. Andrade, R. Ferreira, J. Fabris, R. Domingues, *Biomedical Engineering - Frontiers and Challenges* Intechopen, London **2011**, https://doi.org/10.5772/1019.
[39] H. Unterweger, R. Tietze, C. Janko, J. Zaloga, S. Lyer, S. Dürr, N. Taccardi, O. M. Goudouri, A. Hoppe, D. Eberbeck, D. W. Schubert, A. R. Boccaccini, C. Alexiou, *Int. J. Nanomed.* **2014**, *9*, 3659.
[40] A. K. Gupta, M. Gupta, *Biomaterials* **2005**, *26*, 3995-4021, https://doi.org/10.1016/j.biomaterials.2004.10.012.
[41] D. Dorniani, A. U. Kura, Z. Ahmad, A. Halim Shaari, M. Z. Hussein, S. Fakurazi, *Int. J. Nanomed.* **2012**, *7*, 5745.
[42] L. Li, J. Li, S. Si, L. Wang, C. Shi, Y. Sun, Z. Liang, S. Mao, *Asian J. Pharm. Sci.* **2015**, *10*, 314.
[43] A. Dev, N. S. Binulal, A. Anitha, S. V. Nair, T. Furuike, H. Tamura, R. Jayakumar, *Carbohydr. Polym.* **2010**, *80*, 833-838, https://doi.org/10.1016/j.carbpol.2009.12.040.
[44] H. Thai, C. T. Nguyen, L. T. Thach, M. T. Tran, H. D. Mai, T. T. T. Nguyen, G. D. Le, M. V. Can, L. D. Tran, G. L. Bach, K. Ramadass, C. I. Sathish, Q. V. Le, *Sci. Rep.* **2020**, *10*, 909, https://doi.org/10.1038/s41598-020-57666-8.
[45] O. Alavi, H. Babavalian, F. Shakeri, M. S. Hashemzadeh, M. M. Nemati, *J. Polym. Environ.* **2024**, *32*, 6742-6759, https://doi.org/10.1007/s10924-024-03386-3.
[46] S. Tarafder, K. Nansen, S. Bose, *Mater. Sci. Eng. C* **2013**, *33*, 3121-3128, https://doi.org/10.1016/j.msec.2013.02.049.
[47] A. Mahmood, A. Sharif, F. Muhammad, R. M. Sarfraz, M. A. Abrar, M. N. Qaisar, N. Anwer, M. W. Amjad, M. Zaman, *Int. J. Nanomedicine.* **2019**, *14*, 5397–5413, https://doi.org/10.2147/IJN.S209662.
[48] E. Bertolucci, A. M. R. Galletti, C. Antonetti, M. Marracci, B. Tellini, F. Piccinelli, C. Visone, *IEEE Instrumentation and Measurement Technology Conference* **2015**, *2015*, 1492–1496.
[49] J. K. Patra, G. Das, L. F. Fraceto, E. V. R. Campos, M. P. Rodriguez-Torres, L. S. Acosta-Torres, L. A. Diaz-Torres, R. Grillo, M. K. Swamy, S. Sharma, H. S. Shin, *J. Nanobiotechnol.* **2018**, *16*, 71, https://doi.org/10.1186/s12951-018-0392-8.
[50] M. Rinaudo, *Prog. Polym. Sci.* **2006**, *31* 603–632, https://doi.org/10.1016/j.progpolymsci.2006.06.001.
[51] M. I. Yoshida, M. A. Oliveira, E. C. L. Gomes, W. D. N. Mussel, W. A. Castro, C. D. V. Soares, *J. Therm. Anal. Calorim.* **2011**, *106*, 657–664, https://doi.org/10.1007/s10973-011-1510-0.
[52] W. Wu, Q. He, C. Jiang, *Nanoscale Res. Lett.* **2008**, *3*, 397–404, https://doi.org/10.1007/s11671-008-9174-9.
[53] S. V. Popov, N. Paderin, E. Chistiakova, A. Sokolova, I. Konyshev, V. S. Belozerov, A. Byvalov, *Gels*, **2024**, *10*, 472.
[54] S. C. Dey, M. Al-Amin, T. U. Rashid, M. Z. Sultan, M. Ashaduzzaman, M. Sarker, S. M. Shamsuddin, *IJLRET.*, **2016**, *2*, 52-62.
[55] M. I. Yoshida, M. A. Oliveira, E. C. L. Gomes, W. N. Mussel, W. V. Castro, C. D. V. Soares, *J. Therm. Anal. Calorim.* **2011**, *106*, 657–664.
[56] U. Verma, J. B. Naik, V. J. Mokale, *Am. J. Pharm. Sci. Nanotechnol.* **2014**, *1*, 11-26.
[57] T. Zhang, L. Wang, X. He, H. Lu, L. Gao, *Front. Med.* **2022**, *9*, 799145, https://doi.org/10.3389/fmed.2022.799145.

Manuscript received: March 12, 2025